

DESIGN OF A SUSPENDED CABLE-DRIVEN PARALLEL ROBOT FOR THE SEMI-AUTOMATION OF CONSTRUCTION TASKS

Ethan McDonald¹, Marc Arsenault¹, Steven Beites²

¹*School of Engineering and Computer Science, Laurentian University, Greater Sudbury, ON, Canada*

²*McEwen School of Architecture, Laurentian University, Greater Sudbury, ON, Canada*

Email: emcdonald1@laurentian.ca; marsenault@laurentian.ca; sbeites@laurentian.ca

ABSTRACT

As construction costs continue to rise in Canada, in tandem with a declining supply of skilled trades, housing affordability is becoming a critical concern across the country. This paper presents research on the development of a suspended cable-driven parallel robot (CDPR) as an alternative method of construction designed to semi-automate the assembly of prefabricated panels. The CDPR features parallel cables arranged in pairs that form a series of parallelograms. This cable arrangement restricts the motion of the CDPR's mobile platform to pure translational motion, as long as the cables remain in tension. The paper focuses on the mechanical design of the CDPR, which is developed based on kinematic sensitivity and payload requirements. Details are provided for the design of the frame as well as the cable actuation and routing system, including the selection of actuators. By presenting the design of this CDPR system, this paper contributes to the ongoing effort towards housing affordability with the aim of reducing the costs of construction while addressing the shortages in skilled labour.

Keywords: cable-driven parallel robot; construction; automation; mechanical design; analysis.

CONCEPTION D'UN ROBOT PARALLÈLE SUSPENDU ENTRAÎNÉ PAR CÂBLES POUR L'AUTOMATISATION PARTIELLE DE TÂCHES DE CONSTRUCTION

RÉSUMÉ

Tandis que les coûts de construction ne cessent d'augmenter au Canada et que la main d'œuvre qualifiée se fait de plus en plus rare, l'accessibilité au logement est devenue une source de grande inquiétude. Cet article présente une recherche portant sur le développement d'un robot parallèle suspendu entraîné par câbles (RPEC) en guise de méthode de construction alternative ayant comme objectif l'automatisation partielle de l'assemblage de panneaux préfabriqués. Le RPEC utilise des câbles parallèles agencés en paires pour former une série de parallélogrammes. Cet arrangement des câbles restreint le mouvement de la plate-forme mobile du RPEC à une translation pure tant et aussi longtemps que les câbles demeurent tendus. L'article prête une attention particulière à la conception mécanique du RPEC qui est basée sur la sensibilité cinématique et la charge utile nécessaire. La conception du bâti du RPEC, du système d'actionnement et d'acheminement de ses câbles ainsi que la sélection de ses actionneurs sont discutées. Ce faisant, cet article contribue à l'amélioration de l'accessibilité au logement en visant une réduction des coûts de construction tout en adressant le déficit de main d'œuvre qualifiée.

Mots-clés : robots parallèles entraînés par câbles ; construction ; automatisation ; conception mécanique ; analyse.

1. INTRODUCTION

Housing is one of the greatest challenges across Canada, including the territories and the upper, remote regions of the provinces. Across the country, Canadians struggle to find a safe and affordable place to live due to increased living costs and current practices that are driving up the costs of home ownership. Housing shortages have a detrimental effect on communities, leading to overcrowding, the rapid deterioration of housing stock, unaffordable market rents and potentially homelessness.

The Architecture, Engineering and Construction (AEC) industry has been historically hesitant in adopting novel technologies and therefore operates on traditional methods and materials of construction that unfortunately are driving the cost of housing to unreachable heights. This is further intensified by a declining supply of skilled trades, increased labour costs and short construction seasons in the north. With these issues in mind, the research attempts to confront these barriers through the development of a robotic system to facilitate the assembly of structures based on prefabricated architectural components. The use of robotics in the construction industry is not a novel development [1]. Examples such as: SAM (Semi-Automated Mason) [2]; a robotic bricklaying system designed and engineered to make the bricklaying process safer and less physically demanding, the Winlet glazing robot [3]; a robotic system that assists in the maneuvering and positioning of prefabricated low-order building elements such as windows, and the early research on UAVs (drones) [4]; for the construction of real-scale structures, are all promising applications that have the potential to transform the AEC industry. However, current limitations such as the inability to manoeuvre large objects over great distances, the lack of autonomy or adaptability to existing site conditions, the failure to work alongside a human operator and the difficulties in correcting variances while performing tasks, are all significant factors that lead to apprehension in their adoption.

Through a cross-disciplinary collaboration between robotic engineering and architecture research units, this paper presents the development of a cable-driven parallel robot (CDPR) as an innovative and alternative method for *in-situ* construction. CDPRs consist of a mobile platform (MP) attached to a fixed frame by several cables whose active lengths are controlled by motor-driven winches. The use of cables to displace the MP decreases the inertia of the robot's moving parts, allowing for the potential of higher acceleration motions. Moreover, with significant lengths of cable capable of being stored on the winches, CDPRs have the potential to operate in relatively large workspaces. However, the need for cables to remain in tension at all times poses additional challenges with the design and control of CDPRs.

Employed historically in material/cargo handling applications, high-speed tracking photography and live broadcasting (e.g. Skycam) [5–7], CDPRs have been seldom explored within the AEC industry yet have immense potential to transform current methods of construction. Prior works have proposed the use of CDPRs for curtain wall module installation [8], automated masonry construction [9, 10] and additive manufacturing [11–14]. In a previous work, the authors performed the architectural and geometrical synthesis of a three-degree-of-freedom (3-DoF) translational suspended CDPR with cables arranged into parallelograms based on workspace and kinematic sensitivity requirements [15]. This work is focused on current efforts to develop and build a functional prototype of a similar system for the assembly of structures consisting of structural insulated panels (SIPs).

2. APPLICATION DETAILS AND REQUIREMENTS

The proposed CDPR requires a design that is highly flexible incorporating strength, portability and modularity to ensure the provision of a physical platform for construction. Its target application is for modest structures such as the construction of smaller single family homes, coach houses, etc. This is achieved through pick-and-place operations of prefabricated assemblies composed of SIPs. The CDPR must manipulate panels that measure approximately $2.44 \times 1.22 \times 0.178$ m with a mass of about 60 kg. To achieve this, the CDPR requires 3-DoF in translation and 2-DoF in rotation, with one rotation axis being vertical and the

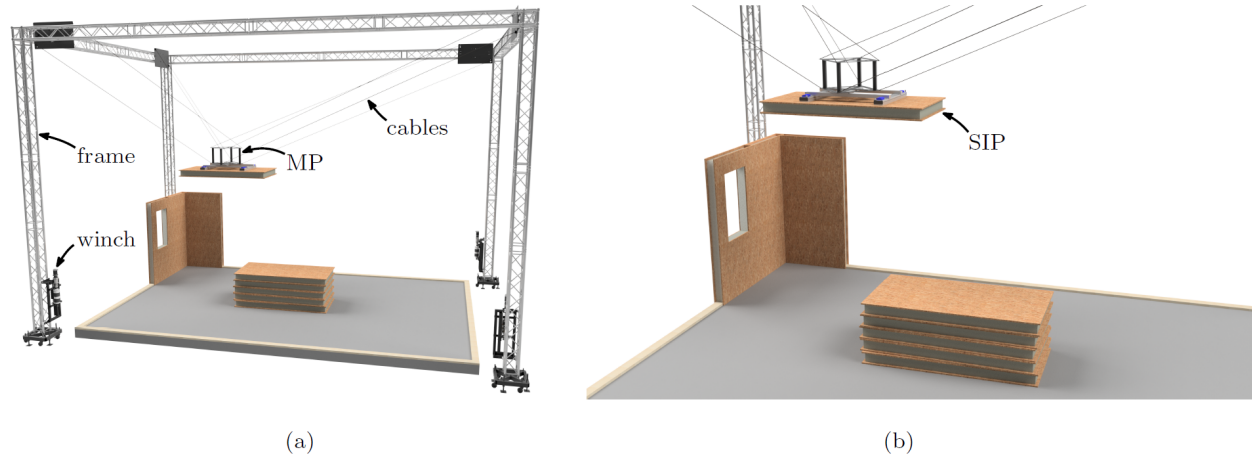


Fig. 1. (a) Wide-angle view of the robot in the intended application and (b) magnified view highlighting the manipulation of the SIPs.

other horizontal. Figure 1 illustrates the CDPR's intended application, showing the robot manipulating a SIP. The targeted CDPR frame is a rectangular prism with length $\ell = 10$ m, width $w = 6.67$ m and height $h = 6.67$ m. Within the region defined by this frame, the proper manipulation of SIPs while avoiding collisions with previously installed units requires the MP to operate at heights reaching $h_{\text{req}} = 4.5$ m. Moreover, the robot must be capable of supporting a maximum expected payload of $m = 100$ kg which includes the mass of a SIP, the MP and any mounted components. Due to the inherent accuracy limitations of CDPRs, the CDPR is intended to initially position the payload in an automated fashion, while a human operator is required for final adjustments to the SIPs, thus acting as a valuable collaborator in the semi-automated assembly process.

The use of a CDPR brings forth several advantages over more traditional methods of construction. It allows for parts of the assembly process to be automated, thus significantly lowering the costs of construction by eliminating the need for highly skilled labour, reducing waste and significantly decreasing construction timelines. It has the ability to extend the construction season in the north where prefab elements can be fabricated in a closed environment during the winter season and installed quickly in the warmer months. As the CDPR automates the positioning and placement of prefabricated assemblies, the human operator remains an important actor in the process. However the need for skilled workers in the building trades is mitigated.

3. ARCHITECTURAL AND GEOMETRICAL SYNTHESIS

As explained in Section 2, the semi-automated construction of structures using SIPs requires 3-DoFs of translation and 2-DoFs of rotation (with one rotation axis being vertical and the other horizontal). Given its ability to operate in large workspaces while manipulating relatively large payloads, a CDPR is chosen to provide the translational motion of a MP. However, due to the limited ability of CDPRs to generate large rotations, it is intended to mount an auxiliary mechanism on the MP in order to reorient the SIPs for assembly. The design of this auxiliary mechanism is beyond the scope of this paper.

When using a CDPR to manipulate SIPs, a critical requirement is to avoid collisions between the cables, the MP or the payload with any objects located in the CDPR's environment. The use of a suspended CDPR architecture mitigates the likelihood of such collisions given that its cables are always located above the payload. Meanwhile, in order to achieve the desired 3-DoFs of translational motion while also constraining the orientation of the MP, the CDPR's cables may be arranged pairwise to form parallelograms, as also

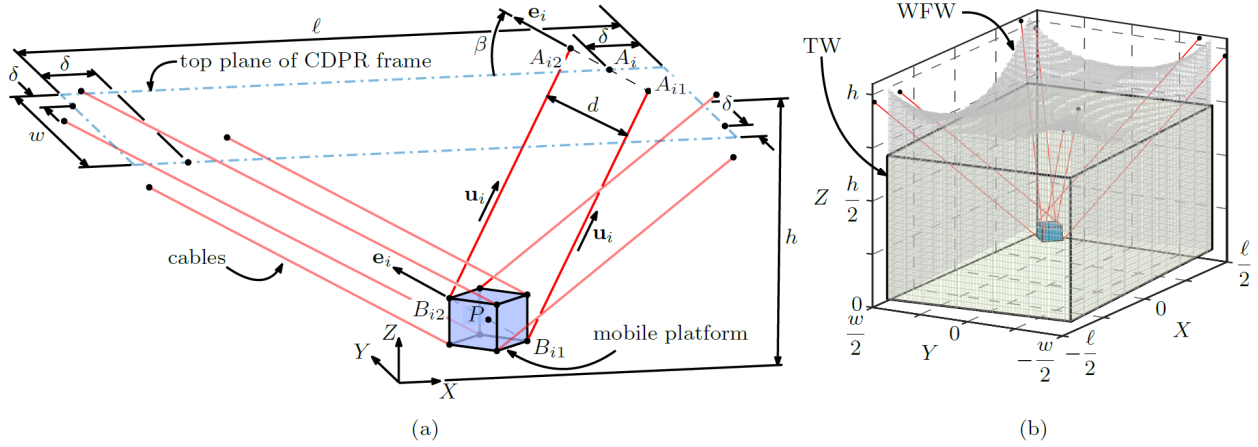


Fig. 2. (a) Schematic representation of the CDPR and (b) illustration of the CDPR's WFW and task workspace.

proposed in *e.g.* [16, 17]. This has the added benefit of reducing the required quantity of actuators since the equal length of cables within a parallelogram may be controlled by a single motor-driven winch unit. Finally, as explained in [15] and also observed in [18], the rectangular footprint of the intended application's desired work area (refer to Section 2) is best achieved by using a total of eight cables arranged in four parallelograms.

Having selected the CDPR architecture, its geometry must now be determined. In [15], an approach was proposed to determine a quasi-optimal CDPR geometry based on performance metrics related to its workspace and kinematic sensitivity. However, the results presented therein are not directly applicable to this work due to constraints on the frame shape and size (refer to Section 2) as well as additional design constraints that result from the methods of assembly used in the development of the CDPR prototype (details are provided in Section 4).

Referring to Fig. 2(a), the j th cable within the i th parallelogram is attached to nodes A_{ij} and B_{ij} on the CDPR's base and MP, respectively ($i = 1, 2, 3, 4$ and $j = 1, 2$). A reference frame XYZ is defined as having its origin O located at the centroid of the bottom of the CDPR's frame, its X axis parallel to the long edge of the frame and its Z axis pointing upward. Nodes A_i , defined as the midpoints of line segments $\overline{A_{i1}A_{i2}}$ (corresponding to the base-attached edges of the cable parallelograms), are located within a plane offset by a height h from the XY plane with position vectors defined as

$$\mathbf{a}_1 = \begin{bmatrix} -\ell + \delta \\ -w \\ h \end{bmatrix}, \quad \mathbf{a}_2 = \begin{bmatrix} \ell \\ -w + \delta \\ h \end{bmatrix}, \quad \mathbf{a}_3 = \begin{bmatrix} \ell - \delta \\ w \\ h \end{bmatrix}, \quad \mathbf{a}_4 = \begin{bmatrix} -\ell \\ w - \delta \\ h \end{bmatrix} \quad (1)$$

Meanwhile, the midpoints of line segments $\overline{B_{i1}B_{i2}}$ (corresponding to the MP-attached edges of the cable parallelograms), denoted as B_i , are chosen to be coincident to the origin P of the $X'Y'Z'$ reference frame (not shown) that is attached to the MP and oriented parallel to the XYZ frame. It may be shown, based on an extension of the proof developed in [15], that this leads to equal cable tensions in the cables of a given parallelogram (and, by association, equal axial deformations of the cables) in the absence of moment loads being applied to the MP. This is key to the CDPR design as the parallelograms defined by the cables are responsible for constraining the MP's motion to pure translation. The remainder of the CDPR's geometry is defined by the width d and orientations of the cable parallelograms. The latter are represented by unit vectors \mathbf{e}_i parallel to line segments $\overline{A_{i1}A_{i2}}$ and $\overline{B_{i1}B_{i2}}$ such that

$$\mathbf{a}_{ij} = \mathbf{a}_i + (-1)^j \frac{d}{2} \mathbf{e}_i \quad \text{and} \quad \mathbf{b}_{ij} = (-1)^j \frac{d}{2} \mathbf{e}_i \quad (2)$$

are the positions of nodes A_{ij} and B_{ij} measured with respect to reference frames XYZ and $X'Y'Z'$, respectively. Both d and \mathbf{e}_i are determined by the pulley system that routes the cables from the actuated winches to the MP (discussed in Section 4.4). To obtain a modular design, the same cable routing system is used for each parallelogram such that

$$\mathbf{e}_i = [-\sin \theta_i \cos \beta \quad \cos \theta_i \cos \beta \quad \sin \beta]^T \quad (3)$$

where $\theta_i = 90(i - 2)$ degrees.

The static equilibrium of the CDPR's MP requires that $\mathbf{W}_p \mathbf{t} = \mathbf{f}$ and $\mathbf{W}_r \mathbf{t} = \boldsymbol{\tau}$ where $\mathbf{t} = [t_{11}, t_{12}, \dots, t_{41}, t_{42}]^T$ is a vector of cable tensions (*i.e.* t_{ij} is the tension in the cable connecting nodes A_{ij} and B_{ij}), \mathbf{f} and $\boldsymbol{\tau}$ are the force and moment, respectively, generated by the MP on its environment while

$$\mathbf{W}_p = [\mathbf{u}_1 \quad \mathbf{u}_1 \quad \cdots \quad \mathbf{u}_4 \quad \mathbf{u}_4] \quad \text{and} \quad \mathbf{W}_r = [\mathbf{b}_{11} \times \mathbf{u}_1 \quad \mathbf{b}_{12} \times \mathbf{u}_1 \quad \cdots \quad \mathbf{b}_{41} \times \mathbf{u}_4 \quad \mathbf{b}_{42} \times \mathbf{u}_4] \quad (4)$$

As shown in Fig. 2(a), \mathbf{u}_i is a unit vector parallel to the i th parallelogram's cables. For the intended application, the only load considered to be applied to the MP for design purposes is the weight of the SIPs such that $\mathbf{f} = [0 \quad 0 \quad mg]^T$, where $g = 9.81 \text{ m/s}^2$. As explained previously, setting $\boldsymbol{\tau} = \mathbf{0}$ leads to $t_i = t_{i1} = t_{i2}$ for the chosen CDPR geometry. Combined with the fact that $\mathbf{b}_{i1} = -\mathbf{b}_{i2}$ (from Eq. (2)) and the definition of \mathbf{W}_r in Eq. (4), $\mathbf{W}_r \mathbf{t} = \mathbf{0}$ is observed to always be satisfied. With the cables in the i th parallelogram sharing the same tension t_i and line of action \mathbf{u}_i , the CDPR's force equilibrium thus simplifies to $\mathbf{W}_0 \mathbf{t}_0 = \mathbf{f}$ where $\mathbf{W}_0 = [\mathbf{u}_1 \quad \mathbf{u}_2 \quad \mathbf{u}_3 \quad \mathbf{u}_4]$ and $\mathbf{t}_0 = 2 [t_1 \quad t_2 \quad t_3 \quad t_4]^T$.

The CDPR's wrench feasible workspace (WFW), defined as the set \mathscr{W} of MP poses where it can generate \mathbf{f} with admissible cable tensions, may be expressed as

$$\mathscr{W} = \left\{ \mathbf{p} \mid \mathbf{W}_0 \mathbf{t}_0 = \mathbf{f}, \quad 0 \leq t_{\min} \leq t_i \leq t_{\max}, \quad \forall i \right\} \quad (5)$$

where $t_{\min} = 0$ is used here whereas t_{\max} is the maximum permissible cable tension based on the CDPR design. In Eq. (5), $\mathbf{p} = [x, y, z]^T$ represents the position of the MP measured in the XYZ frame which, given the fact that the CDPR is designed to undergo pure translational motion, also corresponds to the MP's pose. Given the definition of \mathbf{W}_0 , it may be observed that the WFW does not depend on d or β . With the cable and actuator selection still to come, a target value of t_{\max} is identified based on the application requirements. For this purpose, the CDPR's static workspace (SW) [12] is defined here as the set of MP poses where it can generate \mathbf{f} with non-negative cable tensions. This may be shown to correspond to the set of all MP positions located beneath the quadrilateral defined by the A_i nodes. The subset \mathscr{T} of the SW for which $0 \leq z \leq h_{\text{req}}$ is furthermore defined as the CDPR's task workspace (TW), *i.e.* the region of the Cartesian space in which the MP must be able to move to complete the required tasks. At a given pose of its MP, the maximum required cable tension is obtained when \mathbf{f} is generated using only a subset of three cable parallelograms. It follows that

$$t_{\max} = \max_{\mathscr{T}} \left\{ \max_{i,q} ({}^q t_i) \mid {}^q \mathbf{t}_0 = 2 [{}^q t_1 \quad {}^q t_2 \quad {}^q t_3 \quad {}^q t_4]^T = ({}^q \mathbf{W}_0)^{-1} \mathbf{f} \text{ with } {}^q t_i \geq 0 \quad \forall i \right\} \quad (6)$$

where ${}^q \mathbf{W}_0$ is the subset of \mathbf{W}_0 that is obtained by removing its q th column ($q = 1, 2, 3, 4$). As suggested in Eq. (6), only when a subset of three cable parallelograms is able to generate \mathbf{f} with non-negative cable tensions is it considered in the determination of t_{\max} . Using this approach for the current design scenario yields $t_{\max} = 655 \text{ N}$. As such, if the cable and actuation system are selected so as to be able to (at least) generate t_{\max} , then $\mathscr{T} \subseteq \mathscr{W}$ will hold.

In order to reduce the transmission of errors in the active cable lengths to corresponding errors in the MP pose, d and β may be selected based on the minimization of kinematic sensitivity. For this purpose,

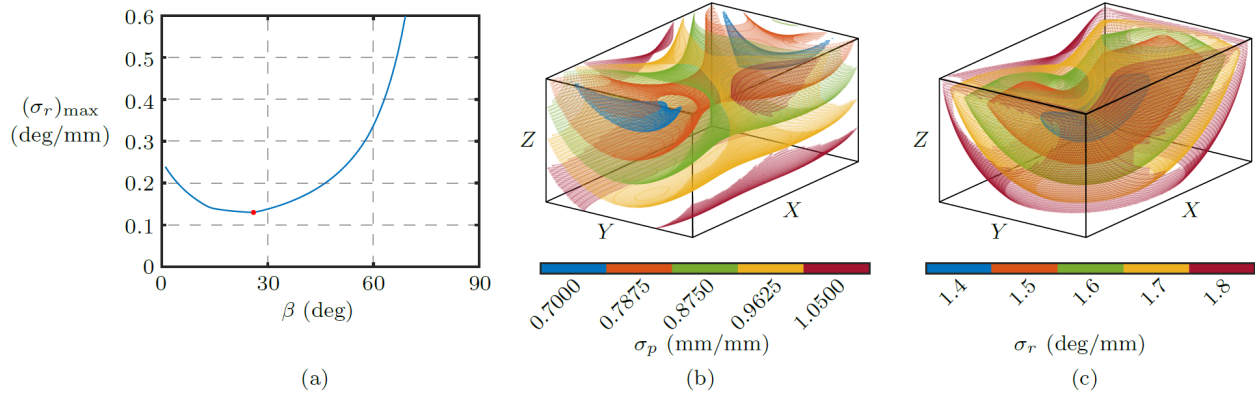


Fig. 3. (a) Plot of $(\sigma_r)_{\max}$ as a function of β as well as the distribution of (b) σ_p and (c) σ_r throughout the CDPR's task workspace.

the CDPR's velocity kinematics are expressed as $\dot{\rho} = \mathbf{J}_p \dot{\mathbf{p}} + \mathbf{J}_r \boldsymbol{\omega}$ where $\dot{\rho} = [\dot{\rho}_1, \dot{\rho}_1, \dots, \dot{\rho}_4, \dot{\rho}_4]^T$ is the 8×1 vector of time rates of change of the cable lengths (note that $\dot{\rho}_i$ applies to both cables within the i th parallelogram), $\boldsymbol{\omega}$ is the angular velocity vector of the MP whereas $\mathbf{J}_p = \mathbf{W}_p^T$ and $\mathbf{J}_r = \mathbf{W}_r^T$ [15]. Applying the method proposed in [19], which has frequently been used to quantify CDPR performance (e.g. [15, 17, 20]), translational and rotational kinematic sensitivity indices are obtained as

$$\sigma_p = \left\{ \min [\text{eig}(\mathbf{J}_p^T \mathbf{J}_p - \mathbf{J}_p^T \mathbf{J}_r (\mathbf{J}_r^T \mathbf{J}_r)^{-1} \mathbf{J}_r^T \mathbf{J}_p)] \right\}^{-\frac{1}{2}} = \left\{ \min [\text{eig}(\mathbf{J}_p^T \mathbf{J}_p)] \right\}^{-\frac{1}{2}} \quad (7)$$

$$\sigma_r = \left\{ \min [\text{eig}(\mathbf{J}_r^T \mathbf{J}_r - \mathbf{J}_r^T \mathbf{J}_p (\mathbf{J}_p^T \mathbf{J}_p)^{-1} \mathbf{J}_p^T \mathbf{J}_r)] \right\}^{-\frac{1}{2}} = \left\{ \min [\text{eig}(\mathbf{J}_r^T \mathbf{J}_r)] \right\}^{-\frac{1}{2}} \quad (8)$$

where $\text{eig}(\cdot)$ returns the eigenvalues of its matrix argument while, given $\mathbf{b}_{i1} = -\mathbf{b}_{i2}$ (refer to Eq. (2)), the fact that

$$\mathbf{J}_p^T \mathbf{J}_r = \mathbf{J}_r^T \mathbf{J}_p = \sum_{i=1}^4 \mathbf{u}_i [(\mathbf{b}_{i1} + \mathbf{b}_{i2}) \times \mathbf{u}_i]^T = \mathbf{0}_{3 \times 3} \quad (9)$$

has been exploited. It may thus be observed from Eq. (7) that σ_p is independent of both d and β . The selection of these parameters is thus based solely on the rotational kinematic sensitivity σ_r . Referring to Eqs. (2) and (4), all elements of $\mathbf{J}_r^T \mathbf{J}_r = \mathbf{W}_r \mathbf{W}_r^T$ are seen to be proportional to d^2 . Given Eq. (8), it follows that $\sigma_r \propto d^{-1}$ such that the CDPR's rotational kinematic sensitivity is decreased by increasing d . In this case, $d = 1$ m is chosen for practical reasons related to the resulting MP size. The optimal value of β , for its part, may be obtained from the following one-dimensional optimization problem

$$\min_{0 < \beta < 90^\circ} \left[(\sigma_r)_{\max} = \max_{\mathcal{T}} (\sigma_r) \right] \quad (10)$$

The solution to Eq. (10), found graphically as illustrated in Fig. 3(a), is $\beta \approx 26$ degrees.

With the design of the CDPR now fully defined, its pose-dependent translational and rotational kinematic sensitivities (i.e. σ_p and σ_r) are plotted throughout the task workspace in Figs. 3(b) and 3(c), respectively. In both cases, expected symmetries about the XZ and YZ planes may be observed. The CDPR's translational kinematic sensitivity is generally better in the upper half of the task workspace where it also tends to improve with distance away from the YZ plane. The rotational kinematic sensitivity, for its part, is best in the central region of the task workspace. It may be shown that the worst case values of both indices throughout the task workspace, which represent the lower bounds of its performance from a kinematic sensitivity perspective, are $(\sigma_p)_{\max} = 1.28$ mm/mm and $(\sigma_r)_{\max} = 0.13$ deg/mm.

4. MECHANICAL DESIGN OF THE CDPR ROBOT

With the robot geometry selected, the mechanical implementation of the CDPR is now discussed in this section. The mechanical design of the CDPR includes several key elements such as selecting a frame and cables, developing a suitable cable actuation system, and routing the cables in such a way that the robot geometry selected in Section 3 is effectively implemented.

4.1. Frame Design

An aluminum truss structure is selected as the frame of the CDPR due to its several advantages. The aluminum truss members are relatively lightweight, which facilitates the assembly and transportation of the frame, and the modular design allows for modifications in the size and shape of the frame as desired. Furthermore, standard components such as clamps, feet, and other accessories are readily available. Aluminum truss structures have previously been implemented in CDPR designs such as the CoGiRo [21].

Truss members with a square cross-section of 290 mm width and constructed using 3 mm wall thickness tubes made of 6082-T6 aluminum alloy are selected as the most cost-effective option while still being capable of supporting the required loads. A preliminary frame is constructed indoors, and it is limited by the size of the room to a size of $4.5 \times 2.5 \times 2.5$ m (length, width, and height). Once possible, the design presented in Section 3 will be assembled outdoors where there are no space constraints to limit the design.

4.2. Cable Selection

Dyneema cables are selected for the CDPR due to their low linear density, which reduces cable sag. Dyneema cables possess other desirable properties including a high strength-to-weight ratio, a low coefficient of friction between itself and many other materials, high axial stiffness, and well documented fatigue properties.

To support the desired 100 kg payload (refer to Section 2), a 2.5 mm Dyneema cable with a tensile strength of 7.1 kN is selected. In Section 3, the maximum required cable tension is found to be $t_{\max} = 655$ N, which is 9.2% of the cable's breaking strength. The number of bending cycles before the cable fails is predicted from results presented in [22], where it is shown that at 9.2% of the cable's breaking strength, it can withstand approximately $6 \cdot 10^5$ bending cycles with a bending ratio (*i.e.*, the ratio of the drum diameter and the cable diameter) of 15. It should be noted that a bending cycle occurs when the cable is either spooled on/off the drum, or is redirected by a pulley. It is therefore important to minimize the number of pulleys used in the cable routing system.

4.3. Cable Actuation System

The cable actuation system (often referred to as a *winch*) consists of a motor-driven drum and a level winding mechanism, and is responsible for controlling the active lengths of each cable to achieve the desired motion of the robot's MP. The selected robot architecture requires pairwise actuation of the cables within a given parallelogram arrangement. The cable actuation system must also be capable of storing the maximum active cable length ρ_{\max} on the drum, and transmit/sustain a cable tension t_{\max} for each cable.

4.3.1. Winding Mechanism

There are generally two main types of winding mechanisms: the spooling-helper mechanism and the rototranslating drum [23]. The spooling-helper mechanism uses pulleys or guides that follow the cable exit point on the fixed drum to ensure that the cable is spooled evenly onto the drum [24]. On the other hand, the rototranslating drum allows the latter to translate, thus keeping the cable exit point constant [25, 26]. The rototranslating drum is advantageous for many applications because it has a constant cable exit point, which makes kinematic modelling simpler [23]. However, rototranslating drums are costly to manufacture

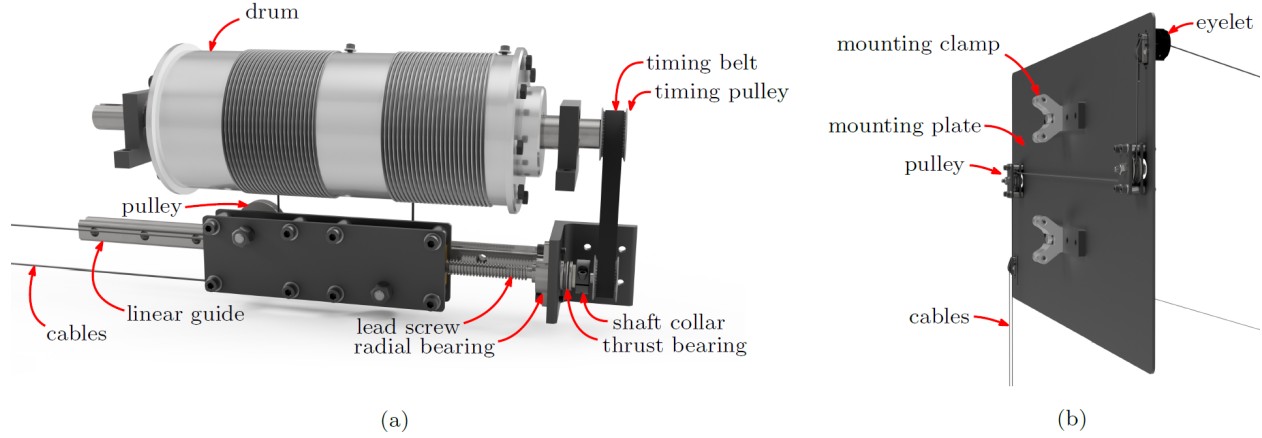


Fig. 4. Renderings of (a) the cable actuation system and (b) the cable routing system.

due to their complexity and high manufacturing tolerance requirements [23]. Thus, the spooling-helper mechanism is selected for the design explored in this paper to prioritize manufacturing efficiency and ease of implementation over a simple kinematic model.

The spooling-helper mechanism shown in Fig. 4(a) consists of two pulleys used to guide each cable onto the drum, mounted to a linear guide and driven by a lead screw. Special attention is given to the placement of the pulleys with respect to the linear guide to minimize the loads transferred to the latter. The lead screw rotation is coupled to the drum rotation through the use of a timing belt and the pitch of the cable wound onto the drum is controlled by changing the drive ratio of the timing pulleys. The cables are routed in a way that always loads the lead screw in tension, preventing buckling and enabling the screw to support a larger thrust load. The lead screw is retained using a redundant system consisting of a shaft collar as the primary retaining component, and a retaining ring as the secondary retaining component. To support the thrust and axial loads and minimize friction within the system, a thrust bearing and a radial bearing are employed.

The drive ratio K relates changes in the i th winch drum's angular position $\Delta q_{d,i}$ to changes in the active cable lengths $\Delta \rho_i$ within the i th ($i = 1, 2, 3, 4$) parallelogram. For a spooling-helper winding mechanism, it is shown in [23] that

$$\Delta \rho_i = K \Delta q_{d,i}, \quad K = \sqrt{K_s^2 + r_d^2} - K_s, \quad K_s = \frac{p}{2\pi} \quad (11)$$

where r_d is the effective drum radius (*i.e.* the distance from the drum's center to the center of the cable) and $p = 3.53$ mm is the pitch of the cable spooled onto the drum, selected to maximize the amount of cable that can be spooled on the drum while avoiding mechanical interference between cables.

4.3.2. Drum

The drum is shown in Fig. 4(a) and is responsible for storing the cable. Drums used in cable actuation systems are either grooved or smooth, with the latter being used in the CDPR design presented in this paper. For prototyping, smooth drums are advantageous because the pitch of the cable stored on the drum can be changed, allowing for different diameter cables to be used, and the drums require less effort to manufacture. However, grooved drums should be used for long term installations to reduced cable wear [23].

The dimensions of the drum are selected to reduce cable wear and to store the required maximum active cable length ρ_{\max} . In [22], it is recommended that a bending ratio (*i.e.* the ratio of the drum diameter to the cable diameter) of 40 or greater be used. Given the diameter of the selected cable is 2.5 mm, the drum diameter should therefore be greater than 100 mm. A drum diameter of 127 mm is selected to exploit the benefits of larger bending ratio while meeting machining constraints. With the cable and drum diame-

ters now selected, $r_d = (127 \text{ mm} + 2.5 \text{ mm})/2 = 64.75 \text{ mm}$, and by substituting all numerical values into Eq. (11), the drive ratio is obtained as $K = 64.19 \text{ mm/rad}$. The required drum length is determined by considering the maximum active cable length ρ_{\max} , which for the CDPR studied in this paper is approximated as $\rho_{\max} = \sqrt{\ell^2 + w^2 + h^2} = 13.75 \text{ m}$, which is the diagonal length of the CDPR's frame. The required number of windings is

$$n_w = \frac{\rho_{\max}}{2\pi K} \quad (12)$$

By substituting all numerical values into Eq. (12), the required number of windings is obtained as $n_w \approx 35$. In [22], it is recommended to add an additional $n_e = 5$ cable windings to significantly reduce the amount of load required to mount the cable to the drum. Since the drum is required to hold two cables, the required drum length is $l_d = 2p(n_w + n_e) = 282.4 \text{ mm}$. When determining the drum length, it is important to account for a system to fix the cables to the drum. To provide sufficient space for cable mounting, the length of the drum is selected as 300 mm.

4.4. Cable Routing System

The cable routing system is responsible for guiding the cables from the winding mechanism pulleys to nodes A_{ij} ($j = 1, 2$) as per the CDPR geometry presented in Section 3.

The cable routing system shown in Fig. 4(b) consists of a series of pulleys used to direct the cables from the cable actuation system, to the eyelets, which are used to implement the A_{ij} nodes to achieve well defined outlets for the cables. The components used in the cable routing system are attached to the mounting plate, which itself is positioned at the top of the aluminum truss structure using mounting clamps.

Each pulley is mounted on a radial bearing to reduce the overall system friction. The cable tension losses in the eyelets are governed by the Euler-Eytelwein formula [22] and thus may be minimized by reducing the cable deflection angle. This can be achieved by aligning the axis passing through the eyelet associated with node A_{ij} with the direction of the cable, defined by \mathbf{u}_i , that is obtained when the MP is centered within the task workspace.

4.5. Mobile Platform and Gripper

With the robot's primary task being to manipulate SIPs, it is important to integrate a gripper into the CDPR design. For the preliminary prototype, Schmalz FXP-SW60 1036 5R18 O10O10 vacuum grippers are used to manipulate SIPs in a horizontal orientation.

Future work on the project will involve the development of an auxiliary mechanism, to be installed between the MP and the vacuum gripper, which will allow for controlling the orientation of the SIPs while in transit. While the robot design discussed in this paper can withstand external disturbance moments, their occurrence is undesirable due to the potential for unequal cable tension within a given parallelogram (see Section 3). To prevent external disturbance moments, it is important to keep the horizontal position of the combined center of mass of the gripper and SIP panel as constant as possible while the panel is being manipulated. This prevents any disturbance moments from acting on the mobile platform, and is therefore one of the primary design goals for the auxiliary mechanism.

5. SELECTION OF ACTUATORS AND CONTROL STRATEGY DEVELOPMENT

5.1. Motor and Gearbox Selection

For the CDPR explored in this paper, the motors used to control the winch must be capable of transmitting at least $t_{\max} = 655 \text{ N}$ cable tension to the segments of cable between nodes A_{ij} and B_{ij} ($i = 1, 2, 3, 4$ and $j = 1, 2$). As the CDPR is intended for use in remote northern communities, it is required that the system can operate off-the-grid using batteries, which means that it can run on direct current (DC) power. The Teknic CPM-SDHP-3446P-ELS servo motors are selected for the CDPR design explored in this paper because the

motors use a standard NEMA 34 mounting system and are DC powered. The selected motors also have an integrated motor driver and an onboard control system that allows the motor to be controlled using step and direction control (*i.e.* the same control method as a stepper motor). As there are no mobile platform speed requirements, the motor selection process is initially based solely on the required motor torque. The chosen motor is capable of outputting $T_m = 2.3 \text{ N}\cdot\text{m}$ of continuous torque at any motor speed. The required gearbox drive ratio is therefore

$$v \geq \sum_{j=1}^2 \frac{t_{\max} r_d}{\eta_e \eta_p^{n_{p,j}} \eta_w \eta_g T_m} \quad (13)$$

where $\eta_p = 0.97$, $\eta_w = 0.8$ and $\eta_g = 0.95$ are lower estimates of the efficiencies of the pulleys, winches and gearboxes, respectively [22]. The quantity of pulleys in the j th cable path is $n_{p,j}$, where, for the selected design (refer to Section 4.4), $n_{p,1} = 2$ and $n_{p,2} = 4$. Finally, $\eta_e = e^{-\mu\phi} = 0.85$ is the efficiency of the eyelets, found using the Euler-Eytelwein formula with an assumed coefficient of friction of $\mu = 0.1$ and a maximum angle between the eyelet axis and the cable of $\phi = 90 \text{ deg}$. Once all numerical values are substituted into Eq. (13), it is found that $v \geq 62.6$. A NEMA 34 gearbox with a drive ratio of $v_g = 70$ is selected as the smallest drive ratio gearbox commonly available on the market that satisfies Eq. (13).

Although a cable speed requirement is not specified, determining the maximum cable speed is still important for trajectory planning and control purposes. The angular velocities of the motors, *i.e.* $\dot{\mathbf{q}} = [\dot{q}_1, \dot{q}_2, \dot{q}_3, \dot{q}_4]^T$, are mapped to the cable velocities as follows

$$\dot{\rho} = K v_g^{-1} \begin{bmatrix} 1 & 1 & 0 & 0 & 0 & 0 & 0 & 0 \\ 0 & 0 & 1 & 1 & 0 & 0 & 0 & 0 \\ 0 & 0 & 0 & 0 & 1 & 1 & 0 & 0 \\ 0 & 0 & 0 & 0 & 0 & 0 & 1 & 1 \end{bmatrix}^T \dot{\mathbf{q}} \quad (14)$$

Although the selected motor may run at speeds up to 185 rad/s, it is capable of generating its peak torque of 9.8 N·m (*i.e.* for the purpose of resisting transient load spikes) at speeds of up to $|\dot{q}|_{\max} = 113 \text{ rad/s}$. The latter is then chosen as the motor's maximum speed of operation from which the maximum cable speed is $|\dot{\rho}|_{\max} = K v_g^{-1} |\dot{q}|_{\max} = 103 \text{ mm/s}$, which, since the MP only moves in translation, also corresponds with the maximum attainable speed of the MP [22].

5.2. Brake Selection

The brakes, located between the motors and the gearboxes, are responsible for preventing uncontrollable movement of the MP in the event of a power failure by resisting against drum rotation. Contrary to the motor selection process, the friction in the system is advantageous and is omitted from the analysis to provide a more conservative estimate of the required brake torque as follows

$$T_b = \frac{2t_{\max} r_d}{v_g} = 1.21 \text{ N}\cdot\text{m} \quad (15)$$

The Newstart MPC034-24-003-T brakes are selected for the CDPR design due to their ability to provide 1.68 N·m of braking torque and their compatibility with NEMA 34 motors.

5.3. Control Strategy

The controller employed in the CDPR is the Teknic ClearCore Controller. This controller receives cable trajectory information from a computer through a serial connection, and subsequently converts this information into step and direction signals that are transmitted to the motors. The integrated controller within the motors processes these signals, determining the required motor position, velocity, and acceleration required to achieve the desired cable trajectory. The onboard controller is propriety and implements a PI control

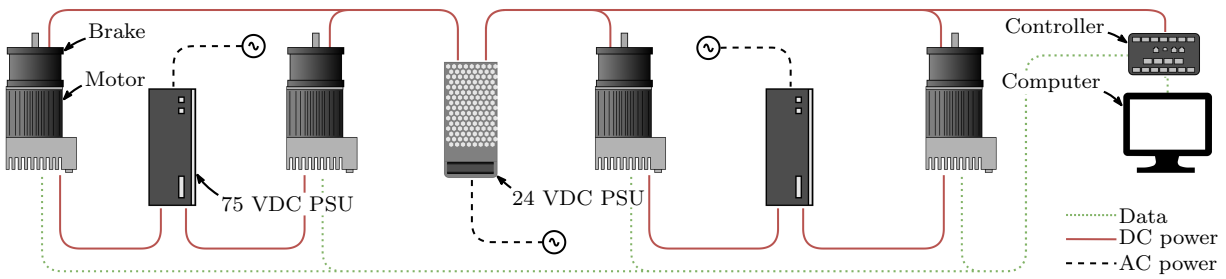


Fig. 5. Motors, brakes and controller integration diagram.

system with an embedded velocity loop and triple-derivative feedforward. Additionally, the controller has the capability to receive signals from the motors, such as motor torque and trajectory tracking errors.

For testing purposes, trajectories are initially generated using parametric equations (*e.g.* the parametric equation representing a circular trajectory in task-space). Once initial testing is complete, trajectories are to be generated using *CDPR Studio*, a CAD-integrated tool under development by the authors that enables simulation and analysis of CDPRs [27].

Figure 5 shows the integration of the controller with the motors, brakes and required power supply units (PSUs). For the preliminary prototype, PSUs are used to power the CDPR using alternating current power. In a future iteration of the CDPR, it is to operate off-the-grid with DC power supplied from batteries.

6. CONCLUSIONS AND FUTURE WORK

This paper has performed the design of a cable-driven parallel robot intended for the semi-automation of construction tasks. A suspended CDPR architecture with its cables arranged pairwise in parallelograms has been selected to minimize cable collisions, constrain the robot's orientation, and reduce the number of required actuators. The robot's geometry has been chosen to optimize its kinematic sensitivity performance and has been implemented through a thorough mechanical design. All key components of the CDPR including the frame, cables, cable actuation system and cable routing system have been designed, and the preliminary prototype is current being assembled indoors.

Future work will involve the construction and testing of the CDPR design presented in this paper, along with the design and implementation of an auxiliary mechanism to reorient the SIPs. Furthermore, the authors plan to continue the development of *CDPR Studio* [27].

REFERENCES

1. Melenbrink, N., Werfel, J. and Menges, A. "On-site Autonomous Construction Robots: Towards Unsupervised Building." *Automation in Construction*, Vol. 119, p. 103312, 2020.
2. Construction Robotics. "Semi-Automated Mason (SAM): Bricklaying Made Simpler and Safer."
3. Hird Ltd. "Winlet Glazing Robots."
4. Goessens, S., Mueller, C. and Latteur, P. "Feasibility Study for Drone-Based Masonry Construction of Real-Scale Structures." *Automation in Construction*, Vol. 94, pp. 458–480, 2018.
5. Brown, G.W. "Suspension System for Supporting and Conveying Equipment, Such as a Camera.", 1986.
6. Qian, S., Zi, B., Shang, W.W. and Xu, Q.S. "A Review on Cable-driven Parallel Robots." *Chinese Journal of Mechanical Engineering*, Vol. 31, No. 1, p. 66, 2018.
7. Cone, L.L. "SKYCAM: An Aerial Robotic Camera System." *Byte*, Vol. 10, No. 10, 1985.
8. Iturralde, K., Feucht, M., Illner, D., Hu, R., Pan, W., Linner, T., Bock, T., Eskudero, I., Rodriguez, M., Gorrotategi, J., Izard, J.B., Astudillo, J., Cavalcanti Santos, J., Gouttefarde, M., Fabritius, M., Martin, C., Henninge, T., Normes, S.M., Jacobsen, Y., Pracucci, A., Cañada, J., Jimenez-Vicaria, J.D., Alonso, R. and Elia, L. "Cable-

- Driven Parallel Robot for Curtain Wall Module Installation.” *Automation in Construction*, Vol. 138, p. 104235, 2022.
9. Bruckmann, T. and Boumann, R. “Simulation and Optimization of Automated Masonry Construction Using Cable Robots.” *Advanced Engineering Informatics*, Vol. 50, p. 101388, 2021.
 10. Herrmann, L., Boumann, R., Lehmann, M., Müller, S. and Bruckmann, T. “Simulation-Based Comparison of Novel Automated Construction Systems.” *Robotics*, , No. 6, p. 119, 2022.
 11. Bosscher, P., Williams, R.L., Bryson, L.S. and Castro-Lacouture, D. “Cable-Suspended Robotic Contour Crafting System.” *Automation in Construction*, Vol. 17, No. 1, pp. 45–55, 2007.
 12. Barnett, E. and Gosselin, C. “Large-Scale 3D Printing with a Cable-Suspended Robot.” *Additive Manufacturing*, Vol. 7, pp. 27–44, 2015.
 13. Izard, J.B., Dubor, A., Hervé, P.E., Cabay, E., Culla, D., Rodriguez, M. and Barrado, M. “On the Improvements of a Cable-Driven Parallel Robot for Achieving Additive Manufacturing for Construction.” In C. Gosselin, P. Cardou, T. Bruckmann and A. Pott, eds., “Cable-Driven Parallel Robots,” *Mechanisms and Machine Science*, pp. 353–363. Springer International Publishing, Cham, 2018.
 14. Chesser, P.C., Wang, P.L., Vaughan, J.E., Lind, R.F. and Post, B.K. “Kinematics of a Cable-Driven Robotic Platform for Large-Scale Additive Manufacturing.” *Journal of Mechanisms and Robotics*, Vol. 14, No. 2, 2021.
 15. McDonald, E., Arsenault, M. and Beites, S. “Design of a 3-DoF Cable-Driven Parallel Robot for Automated Construction Based on Workspace and Kinematic Sensitivity.” *Journal of Mechanisms and Robotics*, Vol. 16, No. 2, March 2023.
 16. Vu, D.S., Barnett, E., Zaccarin, A.M. and Gosselin, C. “On the Design of a Three-DOF Cable-Suspended Parallel Robot Based on a Parallelogram Arrangement of the Cables.” In “3rd International Conference on Cable-Driven Parallel Robots (CableCon),” Vol. 53 of *Mechanisms and Machine Science*, pp. 319–330. Springer Netherlands, Quebec City, Canada, 2018.
 17. Mottola, G., Gosselin, C. and Carricato, M. “Dynamically Feasible Motions of a Class of Purely-Translational Cable-Suspended Parallel Robots.” *Mechanism and Machine Theory*, Vol. 132, pp. 193–206, 2019.
 18. Qin, Z., Liu, Z., Liu, Y., Gao, H., Sun, C. and Sun, G. “Workspace Analysis and Optimal Design of Dual Cable-Suspended Robots for Construction.” *Mechanism and Machine Theory*, Vol. 171, p. 104763, 2022.
 19. Cardou, P., Bouchard, S. and Gosselin, C. “Kinematic-Sensitivity Indices for Dimensionally Nonhomogeneous Jacobian Matrices.” *IEEE Transactions on Robotics*, Vol. 26, No. 1, pp. 166–173, 2010.
 20. Vu, D.S., Barnett, E. and Gosselin, C. “Experimental Validation of a Three-Dof Cable-Suspended Parallel Robot for Spatial Translation with Constant Orientation.” *ASME Journal of Mechanisms and Robotics*, Vol. 11, No. 2, 2019.
 21. Lamaury, J. and Gouttefarde, M. “Control of a Large Redundantly Actuated Cable-Suspended Parallel Robot.” In “2013 IEEE International Conference on Robotics and Automation,” pp. 4659–4664, 2013.
 22. Pott, A. *Cable-Driven Parallel Robots: Theory and Application*, Vol. 120 of *Springer Tracts in Advanced Robotics*. Springer, Cham, Switzerland, 2018.
 23. Idà, E. and Mattioni, V. “Cable-Driven Parallel Robot Actuators: State of the Art and Novel Servo-Winch Concept.” *Actuators*, Vol. 11, No. 10, p. 290. Number: 10, 2022.
 24. Pott, A., Mütterich, H., Kraus, W., Schmidt, V., Miermeister, P. and Verl, A. “IPAnema: A Family of Cable-Driven Parallel Robots for Industrial Applications.” In T. Bruckmann and A. Pott, eds., “Cable-Driven Parallel Robots,” pp. 119–134. Springer Berlin Heidelberg, Berlin, Heidelberg, 2013.
 25. Pham, C.B., Yang, G. and Yeo, S.H. “Dynamic Analysis of Cable-Driven Parallel Mechanisms.” In “Proceedings, 2005 IEEE/ASME International Conference on Advanced Intelligent Mechatronics,” pp. 612–617, 2005.
 26. “A Reconfigurable Robot for Cable-Driven Parallel Robotic Research and Industrial Scenario Proofing.” pp. 135–148. Berlin, Heidelberg, 2013.
 27. McDonald, E., Beites, S. and Arsenault, M. “CDPR Studio: A Parametric Design Tool for Simulating Cable-Suspended Parallel Robots.” In D. Gerber, E. Pantazis, B. Bogosian, A. Nahmad and C. Miltiadis, eds., “Computer-Aided Architectural Design. Design Imperatives: The Future Is Now,” *Communications in Computer and Information Science*, pp. 344–359. Springer, Singapore, 2022.